HHS Public Access

Author manuscript

Eur J Immunol. Author manuscript; available in PMC 2025 January 01.

Published in final edited form as:

Eur J Immunol. 2024 January ; 54(1): e2350561. doi:10.1002/eji.202350561.

Autotaxin in encephalitogenic CD4 T cells as a therapeutic target for multiple sclerosis

Cora L. Petersen-Cherubini[1,2], **Shawn P. Murphy**[2], **Matthew Xin**[2], **Yue Liu**[2], **Joshua L. Deffenbaugh**[2], **Ishrat Jahan**[2], **Christina N. Rau**[2], **Yuhong Yang**[3], **Amy E. Lovett-Racke**[2,4]

[1]The Ohio State University – Neuroscience Graduate Program

[2]The Ohio State University – Wexner Medical Center – Department of Microbial Infection and Immunity

[3]The Ohio State University – Wexner Medical Center – Department of Neurology

[4]The Ohio State University – Wexner Medical Center – Department of Neuroscience

Abstract

Multiple sclerosis (MS) is an immune-mediated inflammatory disease of the central nervous system (CNS). A defining characteristic of MS is the ability of autoreactive T lymphocytes to cross the blood brain barrier (BBB) and mediate inflammation within the CNS. Previous work from our lab found the gene *Enpp2* to be highly upregulated in murine encephalitogenic T cells. *Enpp2* encodes for the protein autotaxin, a secreted glycoprotein that catalyzes the production of lysophosphatidic acid and promotes transendothelial migration of T cells from the blood stream into the lymphatic system. The present study sought to characterize autotaxin expression in T cells during CNS autoimmune disease and determine its potential therapeutic value. Myelin activated CD4 T cells upregulated expression of autotaxin *in vitro*, and *ex vivo* analysis of CNS-infiltrating CD4 T cells showed significantly higher autotaxin expression compared to cells from healthy mice. In addition, inhibiting autotaxin in myelin-specific T cells reduced their encephalitogenicity in adoptive transfer studies and decreased *in vitro* cell motility. Importantly, using two mouse models of MS, treatment with an autotaxin inhibitor ameliorated EAE severity, decreased the number of CNS infiltrating T and B cells, and suppressed relapses, suggesting autotaxin may be a promising therapeutic target in the treatment of MS.

Corresponding author: Amy E. Lovett-Racke, 460 W 12th Ave, Biomedical Research Tower 648, Columbus OH, 43210, amy.lovett-racke@osumc.edu.

AUTHOR CONTRIBUTIONS:

C.L.P-C prepared the manuscript, designed experiments, and collected data with the support of A.E.L-R. Project conceptualization by A.E.L-R., and Y.Y. The following authors contributed to data collection, analysis, and manuscript review: S.P.M., M.X., Y.L., J.L.D., I.J., C.N.R.

ETHICS APPROVAL STATEMENT:

Protocols used in this study were approved by the Institutional Animal Care and Use Committee and Institutional Biosafety Committee at The Ohio State University.

PATIENT CONSENTS STATEMENT: N/A

PERMISSION TO REPRODUCE MATERIAL FROM OTHER SOURCES: N/A

CLINICAL TRAIL REGISTRATION: N/A

CONFLICT OF INTEREST DISCLOSURE: The authors have no conflicts of interest to declare.

Graphical Abstract

Autotaxin is increased by encephalitogenic T cells during EAE. Treatment with an autotaxin inhibitor decreases neurological deficit by reducing T cell motility and infiltration into the CNS.

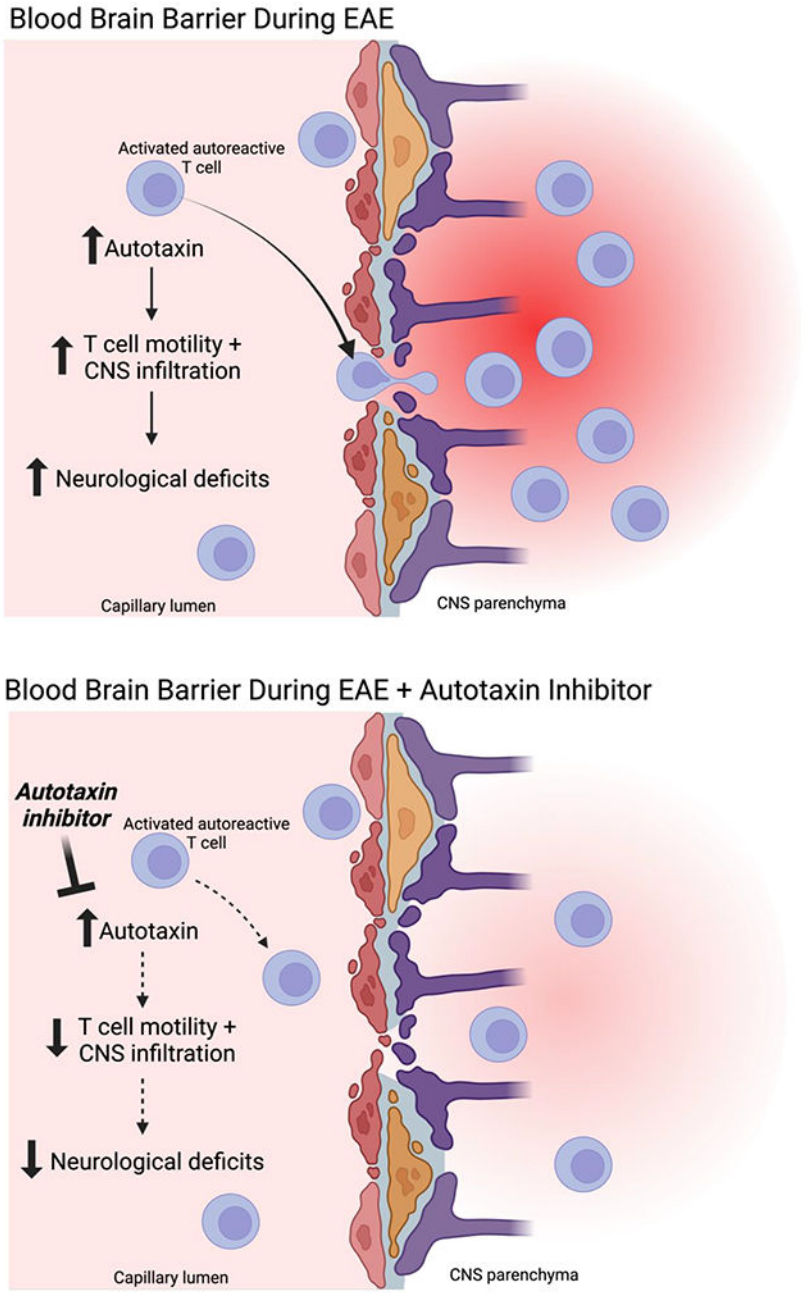

Keywords

autotaxin; autotaxin/LPA axis; CD4 T cells; CNS autoimmunity; multiple sclerosis; experimental autoimmune encephalomyelitis; HA-130

INTRODUCTION:

Multiple sclerosis (MS) is an immune-mediated demyelinating disease of the central nervous system (CNS) facilitated by infiltrating autoreactive T lymphocytes. Although it affects more than 2.8 million people worldwide[1], the precise cause of MS is unknown. To better understand this disease and develop more effective therapies, the molecular mechanisms that directly facilitate the development and trafficking of encephalitogenic T cells must be elucidated.

Utilizing the mouse model of MS, experimental autoimmune encephalomyelitis (EAE), our lab previously determined that the minimum required signals needed to generate encephalitogenic CD4 T cells, in addition to T cell receptor (TCR) and co-stimulation, were two combinations of cytokines: interleukin 6 (IL-6) + IL-23 and IL-12 + IL-23[2]. Since both cytokine combinations require IL-23, gene expression downstream of IL-23 signaling in myelin-specific CD4 T cells was analyzed. One of the genes that was over-expressed by IL-23 encodes the protein autotaxin (ATX), a secreted glycoprotein that catalyzes the production of lysophosphatidic acid (LPA). Once generated, LPA can bind to six known G-protein coupled receptors to facilitate growth-factor like signaling, stimulating migration, survival, and proliferation depending on the number and type of LPA receptors (LPARs) present[3]. Although ATX has a range of functions in local tissues, and is critical during development[4,5], its expression is largely dispensable in adult mice[6], making it a viable therapeutic target. In fact, ATX inhibitors are being evaluated in clinical trials for idiopathic pulmonary fibrosis[7] and metastatic pancreatic cancer[8].

Under healthy physiological conditions, the ATX/LPA axis has direct effects on T cell motility by facilitating lymphocyte homing and T cell egress from the bloodstream into the lymphatic tissue at high endothelial venules (HEVs)[9,10]. Inhibiting this pathway *in vivo* decreases T cell motility within the lymph nodes[11] , and knocking down ATX also decreases dendritic cell migration, suggesting ATX plays an important role in motility of immune cells. LPA can also promote conversion of monocytes into activated macrophages[12]. Thus, ATX signaling is profoundly important for both innate and adaptive immunity.

Recent studies, however, indicate that increased ATX may have negative effects during both systemic and CNS inflammation, and decreasing ATX in these contexts may be clinically beneficial[13,14]. In a mouse model of LPS-induced neuroinflammation, inhibiting ATX or LPA significantly decreased the presence of proinflammatory markers in both the brain and the periphery[13]. A similar effect was seen in a model of hepatic encephalopathy, where there was a significant improvement in both neuroinflammation and neurobehavioral symptoms in ATX inhibitor-treated mice[15]. There have also been several studies investigating the role of ATX in stroke, as increased ATX is seen in the CSF of patients for up to two weeks after stroke[16], and its inhibition or genetic deletion improved outcomes and decreased blood-brain barrier permeability in experimental models[16–18].

In MS patients, ATX is increased in both the cerebrospinal fluid (CSF) and the plasma, but this increase is not seen in patients with other chronic neurological conditions[19]. This observation was supported by another study that found ATX was increased significantly

during first documented MS attack, and in relapsing remitting MS (RRMS) patients[20]. This increase in ATX may contribute to lesion formation, as Nagai et al. showed the catalytic activity of ATX promotes demyelination of *ex vivo* cultured dorsal root fibers[21]. While the cause and origin of excess ATX during MS is unclear, ATX expression has been seen in multiple types of CNS cells, including astrocytes, myeloid cells, and microglia, in response to inflammation or trauma[22,23]. Importantly, knocking out ATX in CD11b+ cells, which include myeloid cells and microglia, decreased severity of EAE, suggesting that ATX expression by innate immune cells contributes to CNS inflammation[23].

In this study, we investigated the potential role of ATX in encephalitogenic T cells in EAE. We found that ATX expression is increased upon antigen stimulation in myelin-specific T cells, as well as in polyclonally activated Th1 and Th17 cells treated with IL-23, a driver of encephalitogenic profile. We show that CNS infiltrating CD4 T cells have increased ATX expression and treating with an ATX inhibitor decreases the pathogenic capacity of these cells by decreasing T cell motility rather than altering activation or cytokine production. Lastly, *in vivo* treatment with an ATX inhibitor at various timepoints of EAE significantly decreases CNS infiltrating immune cells, improves clinical score, and decreases severity of relapses. Taken together, these findings support the idea that ATX may be a viable therapeutic target for MS.

RESULTS:

IL-23 signaling induces autotaxin expression

Since IL-23 is vital to the generation of encephalitogenic T cells[2], we wanted to understand the downstream effects of IL-23 that may be contributing to pathogenicity. Microarray data previously published by our lab showed increased expression of the ATX gene, *Ennp2*, after IL-23 stimulation in murine MBP-specific Th1 and Th17 cells. To confirm these results, RT-qPCR was run on polyclonally activated CD4 T cells from three different mouse strains in the presence of differentiating cytokines. *Enpp2* expression was only increased in Th1 and Th17 cells when cultured in combination with IL-23 (Fig. 1a–c). Polyclonal activation alone, or with individual cytokines, was not enough to raise *Enpp2* mRNA to the same levels. These results validate the microarray data and demonstrate that increased ATX expression by IL-23 in T cells is not a strain-specific observation.

ATX expression is increased by antigen-activated CD4 T cells

It is well established that ATX plays a role in T cell migration and inflammation, predominantly via ATX expression by high endothelial venules[24]. However, a role for ATX expressed by T cells has not been explored. To determine if ATX is expressed in antigen-driven autoreactive T cells, myelin-specific T cell receptor (TCR) transgenic splenocytes were activated *ex vivo* with myelin peptide for three days, a protocol that generates T cells that can induce EAE when injected into naïve mice[25,26]. Since ATX is a secreted protein, intracellular ATX levels were measured by flow cytometry to detect ATX production by CD4 T cells prior to secretion (Fig. 1d). No surface ATX staining was detected, ruling out staining that may be from ATX generated by other cell types. Next, we compared ATX levels in resting T lymphocytes to those activated with antigen (Fig. 1e–g). Negligible

ATX expression was observed in resting T cells (Fig. 1f), but upon activation a population of CD3+ T cells increased ATX expression (Fig. 1g). Further gating on CD25, a marker of T cell activation, shows that this population is primarily made up of activated CD4 T cells. Some activated CD4 T cells were also negative for ATX staining, suggesting ATX expression may be either time-dependent, or a characteristic of a subset of CD4 T cells rather a defining characteristic of activation alone. These data show that ATX expression is increased on the protein level in activated, autoreactive T cells and can be detected intracellularly via flow cytometry.

ATX is increased in CNS infiltrating CD4 T cells

We next asked if ATX is increased in encephalitogenic T cells *in vivo* by analyzing CNS infiltrating T cells during EAE. Brains, spinal cords, spleens, and draining lymph nodes were collected from SJL/J mice, a relapsing-remitting model of MS, with severe neurological deficits following EAE induction (clinical scores of 4, day 16 post immunization), and healthy control mice. Immune cells were isolated from tissues and brought up as single cell suspensions before staining for surface markers and intracellular ATX. EAE mice showed a significant increase in the number of ATX+CD4+ T cells in the spinal cord and brain compared to healthy mice (Fig. 2a–c, f). Interestingly, while ATX+CD4+ T cells were also significantly elevated in the draining lymph nodes nearest the immunization site, this result was not observed in the spleen (Fig. 2d, e). This suggests that the encephalitogenic T cells generated in the draining lymph nodes increase ATX expression, and this increase is maintained when the cells traffic to the CNS. We also investigated changes to ATX+CD4+ populations in the CNS draining lymph nodes but saw no significant differences with EAE (Supplemental Fig. 1). It is well known that ATX is highly expressed in CD11b+ cells during EAE[23]. Our results confirm this finding and we also found there to be no notable increase in ATX in CNS infiltrating B cells (Fig. 2f). Together, these results indicate that ATX expression is increased by select immune cell subsets during EAE and this may be playing a role in CNS inflammation.

ATX inhibition decreases motility and encephalitogenic potential of T cells

HA-130 is a potent (IC_{50}=28nM), boronic acid-based ATX inhibitor that binds to the orthosteric site and decreases turnover and affinity of LPC, the precursor to LPA[27]. To determine if inhibiting ATX affects the ability of cells to become encephalitogenic, we activated myelin-specific TCR transgenic T cells *ex vivo* with myelin peptide in the presence of HA-130 and then transferred the activated myelin-specific T cells into B10.PL mice. Mice that received the HA-130-treated T cells showed decreased disease severity (Fig. 3a), and while all the mice ultimately developed disease, the HA-130 group had prolonged disease-free survival compared to controls (Fig. 3b).

To delineate if the effects of ATX inhibition were due to changes in survival, proliferation, or differentiation, TCR transgenic T cells were similarly activated with antigen in the presence of HA-130. After three days in culture, there were no differences in cell survival as determined by trypan blue viability, or proliferation as determined by ^{3}[H]-thymidine incorporation, compared to vehicle treated cells (Fig. 3c–d). There were also no changes in CD4 T cell activation as assessed by CD25, or intracellular ATX expression determined

by flow cytometry (Fig. 3e). To access if ATX inhibition impacted cytokine production, secreted IFNγ, IL-17 and GM-CSF were analyzed via ELISA. These cytokines were chosen based on their known contributions to encephalitogenicity[28–30]. No difference in GM-CSF or IFNγ secretion was observed in the HA-130 treated T cells (Fig. 3f), and while there was a statistical increase in IL-17 after HA-130, it is likely not physiologically relevant. Alterations in chemokine receptors were also briefly investigated (Supplemental Fig. 2), but there was little change, if any, in most of the molecules analyzed, including CCR2, CCR6, VLA4, PGSL-1, CXCR3 (not shown), CD62L (not shown), and PD-1 (not shown). However, there was notable decrease in the percentage of CD30+ T cells and increase in CCR7+ T cells within the activated CD4 population which may have the potential to decrease trafficking of T cells to the CNS.

Miao et al. showed that addition of ATX to Jurkat cell cultures induces chemokinesis *in vitro*[31]. In contrast, we analyzed whether the ATX produced by activated T cells was sufficient to facilitate motility. To test the hypothesis that HA-130 may be decreasing CNS infiltration by inhibiting chemokinesis, activated myelin-specific T cells were plated in the top well of a transwell plate with vehicle or HA-130. The number of migrated cells significantly decreased with HA-130 treatment (Fig. 3g). This supports the theory that HA-130 treatment may act to decrease CNS infiltration by hindering chemokinesis of activated T cells.

To confirm that HA-130 was inhibiting ATX generated by T cells specifically, CD4+ T cells differentiated into an encephalitogenic Th1 phenotype were polyclonally activated for two days and then replated in serum-free media with vehicle or HA-130 for 24 hrs. Supernatants were collected and screened for ATX activity. HA-130 noticeably decreased ATX activity of cultured T cells ($p=0.0795$) (Fig. 3h), supporting the hypothesis that ATX generated by CD4+ T cells may be contributing to disease.

In combination with the *in vivo* experiments, these data suggest that while treatment with an ATX inhibitor decreases the motility and encephalitogenic potential of myelin-specific T cells, it does not alter T cell survival, proliferation, or cytokine production in response to antigen, all of which are necessary for proper T cell function and host defense *in vivo*.

Treatment with ATX inhibitor decreases clinical severity of EAE at disease onset

Since inhibiting ATX decreases encephalitogenicity, we next asked if treating EAE mice with HA-130 has any clinical benefit. To do this, two different EAE models were treated with HA-130 during different time points of disease. A prior study utilizing a different ATX inhibitor found inhibiting ATX from day one post immunization decreased clinical severity of disease[32]. To determine if inhibiting autotaxin has therapeutic value, HA-130 was administered to mice with established disease. EAE was induced in C57Bl/6J mice and HA-130-infused chow was fed at 10mg/kg or 50mg/kg every day for two weeks beginning when 30% of the mice had developed signs of disease. After ending treatment, the mice were observed for an additional two weeks. There was a significant decrease in clinical score during the treatment period for both doses compared to the vehicle treated mice, but the clinical benefit subsided when treatment was stopped (Fig. 4a). This was likely due to the rapid clearance of HA-130 from circulation as reported by others[27]. While both doses

improved signs of EAE to the same degree, the higher dose of HA-130 (50 mg/kg) provided a slight delay in onset (Fig. 4b), while the lower dose showed less weight loss during treatment (Fig. 4c).

This study was replicated in an experiment in which mice received the drug *i.p.* instead of orally to test for efficacy differences between administration routes. Each mouse began *i.p.* injections 24hr after the onset of clinical signs, and scores are shown normalized to the first day of treatment for each mouse (Fig. 4d–e). The same treatment effect was observed with the two doses of HA-130, and the 50mg/kg group maintained lower scores for longer after the conclusion of the treatment. These data indicate that there is little difference between administration routes, and the effects of ATX inhibition are transient, necessitating continued presence of the inhibitor to have sustained clinical benefits.

Approximately 80-85% of MS patients present with relapsing remitting disease, characterized by periods of active clinical symptoms followed by periods of remission[33]. This phenotype can be modeled in the research setting when EAE is induced in female SJL/J mice[34]. To better determine the clinical benefit of ATX inhibition at different stages of disease, SJL/J mice were treated with HA-130 during the initial acute attack and during the first remission. When mice were treated with 10mg/kg HA-130 or vehicle *i.p.* every day for one week during the initial acute attack, there was a significant improvement in clinical scores compared to control-treated mice, suggesting that inhibiting ATX during the acute phase is beneficial (Fig. 5a). Like in C57Bl/6J mice, this benefit subsided when the drug was no longer administered. When treatment was initiated during the first remission in both active EAE (Fig. 5b) and passively induced EAE (Fig. 5c), relapses were suppressed in the mice treated with HA-130, but like with the other studies, this treatment benefit was lost at the conclusion of treatment. Taken together these data indicate that ATX inhibition after the onset of CNS autoimmunity can decrease the clinical severity of disease and suppress relapses.

Autotaxin inhibition reduces CNS infiltrating CD4 T cells

To elucidate why ATX inhibition improves neurological deficits, the number of CNS infiltrating immune cells were quantified after treatment with HA-130 at 10mg/kg in chow (Fig. 6a). HA-130 treatment significantly decreased the number of CNS infiltrating CD4 T cells in the brain ($p=0.0001$) and spinal cord ($p=0.0582$) compared to vehicle treated mice (Fig. 6b). There was also a notable decrease in B cells in the brain ($p=0.0639$) and spinal cord ($p=0.0657$), that coincided with decreased T cell numbers (Fig. 6c). While there may be a slight reduction in infiltrating myeloid cells of the spinal cord, neither the brain or spinal cord showed statistical significance ($p=0.9013$ and $p=0.5166$, respectively) (Fig. 6d). These data suggest that the benefits observed by HA-130 treatment may be due, at least in part, to reduced T cell-induced neuroinflammation.

Immune cell numbers in the blood and lymph tissue were also assessed to investigate if T cell trafficking was impaired by HA-130 in the context of EAE. Inhibiting ATX caused small fluctuations in immune cell numbers in the injection site draining lymph nodes and the spleen at this timepoint (Fig. 7a–b), but those changes were not significant compared to vehicle treated mice. Interestingly, HA-130 did significantly decrease the number of T

cells (*p=0.0414*) and B cells (*p=0.0127*) in the blood, bringing the levels down to match those seen in healthy controls (Fig. 7c). This effect was not observed in the myeloid cell population. Taken together, these data show that immune cell trafficking and CNS infiltration is significantly altered by inhibiting ATX in EAE.

DISCUSSION:

The present study revealed that ATX expression is increased by T cells that drive CNS autoimmunity and treating with an ATX inhibitor is beneficial at several timepoints during EAE. We provide evidence suggesting that ATX is associated with T cell infiltration into the CNS, highlighting a novel contribution of the ATX/LPA axis to autoimmune pathology and neuroinflammation.

Activated Th1 and Th17 murine T cells increase ATX expression after IL-23 stimulation. Interestingly, HuR, an RNA-binding protein that is involved in the stabilization of ATX Mrna[35] has been implicated in EAE[36] . When HuR is knocked out or pharmacologically inhibited, there is a decrease in blood-brain barrier permeability, EAE severity, and infiltrating immune cells[36,37]. While HuR indirectly affects other pathogenic factors such as T-bet, it directly regulates IL-12Rβ1 expression, which is the shared receptor subunit of IL-12 and IL-23[38]. It is intriguing that inhibiting ATX, one of many downstream targets of this transcription regulator, produces several of the same effects seen with global knockout or inhibition of HuR itself. Future study needs to be done to determine the role of HuR in promoting ATX expression downstream of IL-23 signaling in CD4 T cells.

Thirunavukkarasu *et al.* found that treatment with a different ATX inhibitor decreased clinical EAE when dosed orally, twice daily, at 30mg/kg beginning at the day of immunization[32]. While this poses interesting implications for disease prevention, in clinical practice, MS patients do not begin therapeutic intervention until after they meet strict diagnostic criteria[39]. For this reason, our study focused on treating animals with established disease rather than beginning treatment the same day as immunization. Here, we find that inhibiting ATX is beneficial in active EAE of C57Bl/6J mice when administered after onset of disease, both *i.p.* and orally, at doses up to 50mg/kg. We also show that HA-130 decreases relapse severity in both active and passively induced EAE in the SJL/J model, which has not been previously examined. Lastly, we show that HA-130 decreases CNS infiltrating T cells and reduces T cell motility *in vitro*, highlighting a novel role of ATX in promoting T cell encephalitogenicity during EAE.

LPA, the product of ATX signaling, induces rapid, but reversible, blood-brain barrier permeability in a concentration-dependent manner[40]. In a mouse model of ischemic stroke, HA-130 was found to rescue blood-brain barrier integrity by decreasing LPA levels and supporting maintenance of tight junction proteins[18]. There is no evidence to suggest that HA-130 directly crosses the blood-brain barrier, so this study focuses on the effects it has on peripheral immune cell infiltration, with the caveat that HA-130 may be able to enter the CNS at sites where the blood-brain barrier is compromised, such as lesions. With that in mind, there are a few possibilities as to why HA-130 may decrease EAE severity that go beyond global inhibition of LPA.

Multiple studies have shown that HA-130 prevents lymphocyte egress across high-endothelial venules, suggesting that inhibiting the enzymatic activity of ATX has direct consequences on T cell trafficking[9,10]. In fact, HA-130 has been shown to decrease the ATX-induced motility of T cells through suppression of the FAK/Src signaling pathway[31]. Our results show that pre-treatment of autoreactive CD4 T cells *in vitro* with HA-130 reduces the severity of disease in our adoptive transfer model. Therefore, one theory is that ATX inhibition may prime encephalitogenic T cells to be less motile when transferred into recipient mice, which may impede CNS infiltration. In support of this theory, Zhang et al 2012 found that pretreatment of lymphocytes with ATX leads to effective transmigration of T cells across a monolayer of endothelial cells in the presence of LPC[9]. In our study, we found that inhibiting the ATX generated by myelin-activated T cells decreases this motility. Of note, several current therapies for MS interfere with ATX signaling on T cells as well. Fingolimod, a sphingosine I-phosphate (S1P) receptor modulator, blocks T cell egress from the lymph nodes by preventing S1P signaling. ATX, in addition to catalyzing the majority of systemic LPA, regulates S1P production and is competitively inhibited by Fingolamod[41]. Another common therapy, Natalizumab, is a monoclonal antibody that binds to α4β1 integrins to prevent T cells from trafficking to the CNS[41]. ATX also binds the same integrins to generate LPA in close vicinity to its receptors on the surface of T cells, which may contribute to extravasation[42,43]. Thus, competition for this integrin binding by Natalizumab may hinder local LPA production and therefore contribute to decreased T cell trafficking. Taken together, these studies support the notion that ATX inhibition influences T cell motility, directly or indirectly, and this may be contributing to improved clinical outcomes seen in EAE. Mechanistic studies of HA-130 on encephalitogenic T cell trafficking need to be run to confirm this hypothesis.

While we show that ATX+CD4+ T cells are more abundant in the CNS of EAE mice compared to controls, we cannot rule out the impact of inhibiting ATX/LPA produced by other cell types. As previously determined, there is evidence to suggest that ATX derived from myeloid cells and microglia may be negatively contributing to EAE[23]. ATX is also highly expressed by astrocytes after neurotrauma[22]. In a model of neuropathic pain, inhibiting ATX shows clinical benefit and decreased presence of activated microglia and astrocytes[44]. Thus, in addition to cell-specific effects, HA-130 may be helping reduce EAE signs by decreasing the neuroinflammation associated with ATX production by glia and infiltrating myeloid cells. Of note, ATX plays a role in oligodendrocyte differentiation during development in zebrafish[5,45]. While it is unclear what role ATX plays in myelin regeneration in the adult brain after neurotrauma or inflammation, the contribution of ATX to and from these various cell types should be considered in future studies.

Like high-endothelial venules, ATX is also highly expressed in the brain[43,46]. The choroid plexus, a vascular network comprised of specialized cells that surround the ventricles, secretes robust amounts of ATX into the CSF[47]. Not only is the choroid plexus an important site for immune surveillance[48,49], but it is also an entry point for activated Th1 cells[48] and Th17 lymphocytes during early EAE[50]. The mechanism behind immune surveillance and trafficking at this site is limited, though with high local levels of ATX, it is conceivable that ATX may be playing a role in T cell infiltration at the choroid plexus in a manner similar to that observed in peripheral high-endothelial venules. Thus, another possible theory for

the clinical benefit of ATX inhibition in EAE may be to impede signaling at this local cell milieu.

Naïve T cells primarily express LPA receptors 2, 5 and 6[51]. Of note, LPAR2 is involved in immune cell homing to the spleen during EAE[20], but the contribution of LPAR2 to inflammation seems to vary based on immunological context. Genetic deletion of LPAR2 has no effect on LPS-induced sepsis[14] suggesting that the presence of LPAR2 on T cells is not necessary to fight systemic infection. Interestingly, while global knockout of this receptor in EAE led to worse clinical symptoms, inhibiting LPAR2 therapeutically was clinically beneficial[20]. This suggests that LPAR2 may be important to multiple cell types during EAE but blocking it in circulation may be specifically helpful during autoimmunity as opposed to infection. These findings support our hypothesis that inhibiting the ATX/LPA axis may be advantageous in the context of MS.

The molecular drivers of encephalitogenic T cells in MS and EAE remain uncertain. Our research has found that ATX, a secreted glycoprotein that is involved in facilitating the motility and extravasation of T cells, contributes to encephalitogenicity in the mouse model of MS. Through gene expression analysis, we have identified the proinflammatory cytokine IL-23 as an important regulator of ATX expression in CD4 T cells. We find increased ATX on T cells in the brain, spinal cord, and lymph node cells of EAE mice, but no significant difference on those in the spleen. Additionally, we show that inhibiting ATX decreases the encephalitogenic potential of T cells without hindering T cell survival, proliferation, or cytokine production, and *in vivo* inhibition provides significant clinical benefit during three different timepoints of EAE. Taken together, these data suggest a role of ATX in driving CNS inflammation and that its inhibition should be further evaluated in the treatment of MS.

MATERIALS AND METHODS:

Mouse Studies

Experimental autoimmune encephalomyelitis (EAE) was induced in C57Bl/6J mice (Jackson Laboratory) and SJL/J mice, age 8-15 weeks. Complete Freud's Adjuvant with 4mg/mL crushed, deactivated mycobacterium tuberculosis and 1mg/mL myelin peptide [MOG 35-55 (C57Bl/6) or PLP139-151 (SJL/J)] were emulsified and injected subcutaneously above shoulders and hips of anesthetized mice, 50μL per injection site for a total of 200μL emulsion. For studies using C57Bl/6J mice, pertussis toxin (List Labs, 50μg/mL) in 200μL PBS was diluted to 200-400ng depending on lot potency and injected intraperitoneal (*i.p.*) on the day of immunization (day 0) and two days post-immunization (day 2). Mice were then monitored for signs of EAE beginning on day 9 post-immunization. EAE scores defined as follows: 0- no clinical signs, 1- limp tail, 2- moderate hindlimb weakness, 3- severe hindlimb weakness, 4- complete hindlimb paralysis, 5- quadriplegia, and 6- deceased due to EAE. All animal studies were conducted in accordance with The Institutional Animal Care and Use Committee protocols at The Ohio State University.

For adoptive transfer studies, splenocytes from a TCR Vα2.3 Vβ8.2 transgenic mouse, which recognize MBP Ac1-11[52], were cultured with 10 μg/mL MBP Ac1-11 in the presence of irradiated B10.PL feeder cells and 1μM HA-130 (Calbiochem) or vehicle for 3 days. The

cells were then washed with PBS and $5X10^6$ cells were injected *i.p.* into WT B10.PL mice. Clinical monitoring began three days after injection.

HA-130 preparation and treatment

Lyophilized HA-130 (Calbiochem) was purchased in 10mg vials and reconstituted in dimethyl sulfoxide at 50mg/mL and stored at −20°C until use. For *i.p.* injections, HA-130 in the specified dose was diluted in sterile PBS. Polyethene glycol 200 (PEG 200) was added to increase solubility of the drug, and the injection volume for each mouse was 200μL/day. Vehicle treated mice received *i.p.* injections of DMSO, PEG 200, and PBS in the same doses as HA-130 treated mice. Drug-treated chow was made in one-week intervals. HA-130 or vehicle, at 10mg/kg or 50mg/kg, was evenly distributed on pellets using 100% ACS-grade ethanol in a chemical hood. Ethanol was allowed to evaporate, and then treated chow was placed in the food hopper and in a petri dish on the floor of the cage to ensure accessibility for all diseased mice. *In vitro* studies were conducted with 1μM of HA-130 diluted from stock in DMSO.

Flow cytometry

For *ex vivo* analysis of murine lymphocytes, single cell suspensions were generated from spleens and lymph node. Axillary, brachial, and inguinal lymph nodes were pooled for isolation. Our flow cytometry protocols adhered to the standards as described in Cossarizza *et al.*[53]. Cells were blocked in 1% BSA/PBS with FC block for 15 mins prior to the addition of antibodies (Supplemental Table 1). Antibodies were added to cells for 30 mins at room temperature (RT) before washing three times with 1% BSA/PBS. Cells were then fixed with Fixation/Permeabilization solution (BD Biosciences) for 20 mins on ice. Cells were washed three times with 1X BD Perm/Wash™ buffer before adding FC block and primary non-conjugated rabbit anti-mouse/human ATX antibody (LS Biosciences). Cells were incubated at RT for 1hr then washed three times with 1X Perm/Wash™ buffer. Rabbit IgG APC-conjugated secondary antibody (R&D Systems) with FC block was then added for 30mins at RT before washing three final times and resuspending in 0.5% formaldehyde.

Samples were run on BD FACSymphony™ A3 Cell Analyzer and processed with FlowJo™ v10.8.1 Software (BD Life Sciences). Statistical analysis was performed with GraphPad Prism version 9.3.0 for Mac OS, GraphPad Software, San Diego, California USA, www.graphpad.com

Isolating CNS infiltrating immune cells

Healthy or EAE mice were euthanized with CO_2, and brain and spinal cords were collected in sterile PBS. Samples were added to 2mL digestion buffer (2.5mg/mL collagenase with 10μg/mL DNase in PBS), and incubated at 37°C for 45 mins, with shaking every 15 mins. Samples then passed through a 70μm cell strainer and washed with 8mL PBS. Cells were recovered by centrifugation at 1500rpm for 5 mins and resuspended in 6mL of 38% Percoll® before centrifuging again at 2000rpm for 30 mins. Supernatant was removed and the cell pellet resuspended in 2mL PBS. Cells were washed once more with PBS and then brought up as a single cell suspension and stained for flow cytometry.

ELISAs

Immulon™ 2 HB Flat Bottom Microtiter Plates (ThermoFisher) were coated with 2μg/mL of capture antibody for murine IFNγ (BD Biosciences), IL-17 (eBioscience), GM-CSF (R&D Systems) and refrigerated overnight. Plates were washed twice with 0.05% Tween 20 in PBS and blocked for 1hr with 200μL 1% BSA/PBS. Supernatants were collected from samples after three days in culture and diluted with PBS before 100uL was added to ELISA plates. Two-fold dilutions were made from recombinant murine IFNγ, IL-17, GM-CSF and 100uL added to plates in the following concentrations: 2, 1, 0.5, 0.25, 0.125, 0.063, 0.031, or 0ng/mL. All samples and standards were plated in triplicate. Plate refrigerated overnight and washed 4 times with PBS/0.05% Tween the following day. Biotin-conjugated detection antibodies were added to plates at 1μg/mL for 1hr at RT. Plates washed six times with PBS/0.05% Tween and 2.5μg/mL avidin-peroxidase (Millipore Sigma) added for 30mins at RT. Plates were washed six times with PBS/0.05% Tween and 100μL 3,3′,5,5′-Tetramethylbenzidine solution (Millipore Sigma) added for 5-15 mins until color developed. Reaction was quenched with 100uL 2N H_2SO_4 and plates read on Molecular Devices Emax Precision Plate Reader at 450nm. Softmax® Pro version 5.0 (Molecular Devices) was used to process plate, and data was analyzed in Excel. GraphPad Prism version 9.3.0 for Mac OS was used to generate graphs and run statistical analysis. Values were defined as significant if $p \leq 0.05$.

CD4+ T cell isolation and RT-qPCR

After collecting cultured cells and washing once with PBS, CD4+ T cells were isolated using MojoSort™ Mouse CD4 T Cell Isolation Kit (Biolegend), then resuspended in Trizol (Life Technologies) and stored at −80°C. RNA was isolated and measured with NanoDrop (Thermo Scientific) before generating cDNA according to the Superscript™ III kit protocol (Invitrogen). RT-qPCR plates (384-well) were loaded with 80-100ng cDNA, 5μL Universal Taqman® PCR Master Mix (Applied Biosystems) and 0.5μL mouse *Enpp2* TaqMan® Primer (Thermo Fisher Scientific, Mm00516572_m1), with 0.5μL water. Each sample was plated in duplicate and HPRT1 was used as an endogenous loading control. Plate was processed in the OSU Cancer Genomics Core Facility. RQ values represent $2^{-\Delta\Delta CT}$ values calculated from endogenous loading control in Excel and visualized with GraphPad Prism.

[3H] Thymidine Incorporation Assay:

Murine splenocytes were isolated and plated in quadruplicate on a 96 well plate. 100,000 cells were activated with 1μg/mL of plate bound anti-CD3/CD28 (BD Biosciences) or MBP Ac1-11 at 10μg/mL. HA-130 (1μM) and/or specified cytokines were added to the cells before culturing for three days at 37°C. On day three, 30μL of [^{3}H]-thymidine (10μCi/mL) in cell culture media was added to the plate and cells were incubated overnight at 37°C. Cells were harvested on filter plates and thymidine incorporation was measured using TopCount® NXT™ Microplate Scintillation and Luminescence Counter (Perkin Elmer). Data analyzed with GraphPad Prism 7.

Transwell Migration Assay

Myelin-specific splenocytes from TCR Vα2.3 Vβ8.2 mice were plated 1:10 with WT B10.PL splenocytes and activated with 10μg/mL MBP Ac1-11 for 24hr. HA-130 (1μM) was added to cells the day before collection, and then cells were replated in serum free media (RPMI-1640 with HEPES) in the top well of a Transwell® plate (0.5μm pore size, Corning). HA-130 (1μM) or vehicle was added to the top well with the cells in 100μL total volume, and 600 μL serum free media was added to the bottom well. Samples were incubated for 20hr in incubator, and then cells that migrated into the bottom well were collected and counted with Vi-CELL BLU Cell Viability Analyzer (Beckman Coulter). Samples ran in triplicate, mean ± SEM, Unpaired T test with Welch's correction. All data representative of two independent experiments.

Autotaxin Activity Assay

Splenocytes were collected from 4 WT C57Bl/6 mice and CD4+ T cells were isolated using mouse CD4+ T Cell Isolation kit (Miltenyi Biotec) according to the manufacturer protocol. Purity of cells was checked by flow cytometry and samples had >97% purity. T cells were plated in 48 well plates at $1x10^6$ cell/well and activated with Dynabeads™ Mouse T-Activator CD3/CD28 beads (Gibco) at 1:10 (beads:cells). Recombinant mouse IL-12 (R&D Systems) and recombinant mouse IL-23 (R&D Systems) were added to the culture at 0.5ng/mL and 5ng/mL, respectively, and cells were incubated for 48hr. Samples were collected, washed once, and replated in serum free media for 24hr with either vehicle or HA-130 (1 μM). Supernatants were then collected, and an Autotaxin Activity Assay (Eschelon Bioscience) was run. Manufacturer protocol was followed for sample addition and plate set up, and then plate was read using SpectraMax® M2 plate reader (Molecular Devices). Plate reader was set to 37°C with an excitation of 485nm and emission at 528nm. Plate was read 6 times/well every 2mins for 2hrs. Data analysis performed using the Excel spreadsheet provided by Eschelon Bioscience and is reported in "ATX Units" defined by the manufacturer as "pM FS-3 hydrolyzed/min in 10 μM FS-3, 50 mM Tris-Cl pH 8.0, 5 mM KCl, 1 mM CaCl2, 1 mM MgCl2, 140 mM NaCl, 1 mg/ml Fatty Acid Free BSA, 1 mM LPC at 37°C". Samples were run in duplicate and data represent two independent experiments.

Statistics

Statistical analysis was performed in GraphPad Prism 7 and all tests are denoted in the figure legends. Welch's T test was used to analyze data comparing two groups, with pairing applied when appropriate. Mann-Whitney test was applied for all clinical EAE data to compare individual treatment groups to the control/vehicle treated group. Values were defined as significant if $p \leq 0.05$.

Supplementary Material

Refer to Web version on PubMed Central for supplementary material.

FUNDING STATEMENT:

The work presented in this study was funded by the National Institute of Health, project number 5R01AI140741.

DATA AVAILABILITY STATEMENT:

The data that support the findings of this study are available from the corresponding author upon reasonable request.

Abbreviations:

ATX	autotaxin
MS	multiple sclerosis
EAE	experimental autoimmune encephalomyelitis
CNS	central nervous system
BBB	blood brain barrier
TCR	T cell receptor
LPA	lysophosphatidic acid
LPARs	LPA receptors
HEVs	high endothelial venules
CSF	cerebrospinal fluid
IL	interleukin

References

(1). Walton C; King R; Rechtman L; Kaye W; Leray E; Marrie RA; Robertson N; La Rocca N; Uitdehaag B; van der Mei I; Wallin M; Helme A; Angood Napier C; Rijke N; Baneke P Rising Prevalence of Multiple Sclerosis Worldwide: Insights from the Atlas of MS, Third Edition. Multiple Sclerosis Journal 2020, 26 (14), 1816–1821. 10.1177/1352458520970841. [PubMed: 33174475]

(2). Lee PW; Smith AJ; Yang Y; Selhorst AJ; Liu Y; Racke MK; Lovett-Racke AE IL-23R-Activated STAT3/STAT4 Is Essential for Th1/Th17-Mediated CNS Autoimmunity. JCI Insight 2017, 2 (17). 10.1172/jci.insight.91663.

(3). Yung YC; Stoddard NC; Chun J LPA Receptor Signaling: Pharmacology, Physiology, and Pathophysiology. Journal of Lipid Research. American Society for Biochemistry and Molecular Biology Inc. 2014, pp 1192–1214. 10.1194/jlr.R046458. [PubMed: 24643338]

(4). van Meeteren LA; Moolenaar WH Regulation and Biological Activities of the Autotaxin-LPA Axis. Progress in Lipid Research. March 2007, pp 145–160. 10.1016/j.plipres.2007.02.001. [PubMed: 17459484]

(5). Yuelling LW; Waggener CT; Afshari FS; Lister JA; Fuss B Autotaxin/ENPP2 Regulates Oligodendrocyte Differentiation in Vivo in the Developing Zebrafish Hindbrain. Glia 2012, 60 (10), 1605–1618. 10.1002/glia.22381. [PubMed: 22821873]

(6). Katsifa A; Kaffe E; Nikolaidou-Katsaridou N; Economides AN; Newbigging S; McKerlie C; Aidinis V The Bulk of Autotaxin Activity Is Dispensable for Adult Mouse Life. PLoS One 2015, 10 (11). 10.1371/journal.pone.0143083.

(7). Maher TM; Kreuter M; Lederer DJ; Brown KK; Wuyts W; Verbruggen N; Stutvoet S; Fieuw A; Ford P; Abi-Saab W; Wijsenbeek M Rationale, Design and Objectives of Two Phase III, Randomised, Placebo-Controlled Studies of GLPG1690, a Novel Autotaxin Inhibitor, in Idiopathic Pulmonary Fibrosis (ISABELA 1 and 2). BMJ Open Respir Res 2019, 6 (1). 10.1136/bmjresp-2019-000422.

(8). Lahn M A Study to Assess an ATX Inhibitor (IOA-289) in Patients With Metastatic Pancreatic Cancer. https://clinicaltrials.gov/ct2/show/NCT05586516#contacts.

(9). Zhang Y; Chen Y-CM; Krummel MF; Rosen SD Autotaxin through Lysophosphatidic Acid Stimulates Polarization, Motility, and Transendothelial Migration of Naïve T Cells. J Immunol 2012, 189 (8), 3914. 10.4049/jimmunol.1201604. [PubMed: 22962684]

(10). Bai Z; Cai L; Umemoto E; Takeda A; Tohya K; Komai Y; Veeraveedu PT; Hata E; Sugiura Y; Kubo A; Suematsu M; Hayasaka H; Okudaira S; Aoki J; Tanaka T; Albers HMHG; Ovaa H; Miyasaka M Constitutive Lymphocyte Transmigration across the Basal Lamina of High Endothelial Venules Is Regulated by the Autotaxin/Lysophosphatidic Acid Axis. The Journal of Immunology 2013, 190 (5), 2036–2048. 10.4049/jimmunol.1202025. [PubMed: 23365076]

(11). Katakai T; Kondo N; Ueda Y; Kinashi T Autotaxin Produced by Stromal Cells Promotes LFA-1–Independent and Rho-Dependent Interstitial T Cell Motility in the Lymph Node Paracortex. The Journal of Immunology 2014, 193 (2), 617–626. 10.4049/jimmunol.1400565. [PubMed: 24935929]

(12). Ray R; Rai V Brief Report Lysophosphatidic Acid Converts Monocytes into Macrophages in Both Mice and Humans. 2017. 10.1182/blood-2016-10.

(13). Joshi L; Plastira I; Bernhart E; Reicher H; Triebl A; Köfeler HC; Sattler W Inhibition of Autotaxin and Lysophosphatidic Acid Receptor 5 Attenuates Neuroinflammation in Lps-activated Bv-2 Micro-Glia and a Mouse Endotoxemia Model. Int J Mol Sci 2021, 22 (16). 10.3390/ijms22168519.

(14). Nikitopoulou I; Katsifa A; Kanellopoulou P; Jahaj E; Vassiliou AG; Mastora Z; Dimopoulou I; Orfanos SE; Aidinis V; Kotanidou A Autotaxin Has a Negative Role in Systemic Inflammation. Int J Mol Sci 2022, 23 (14). 10.3390/ijms23147920.

(15). Roy S; Chakrabarti M; Dasgupta H; Mahale A; Tripathi S; Sharma V; Banerjee M; Kulkarni OP Inhibition of Autotaxin Ameliorates LPA-Mediated Neuroinflammation and Alleviates Neurological Dysfunction in Acute Hepatic Encephalopathy. ACS Chem Neurosci 2022, 13 (19), 2829–2841. 10.1021/acschemneuro.2c00046. [PubMed: 36112416]

(16). Bitar L; Uphaus T; Thalman C; Muthuraman M; Gyr L; Ji H; Domingues M; Endle H; Groppa S; Steffen F; Koirala N; Fan W; Ibanez L; Heitsch L; Cruchaga C; Lee J-M; Kloss F; Bittner S; Nitsch R; Zipp F; Vogt J Inhibition of the Enzyme Autotaxin Reduces Cortical Excitability and Ameliorates the Outcome in Stroke; 2022; Vol. 14. https://www.science.org.

(17). Bhattarai S; Subedi U; Manikandan S; Sharma S; Sharma P; Miller C; Bhuiyan MS; Kidambi S; Aidinis V; Sun H; Miriyala S; Panchatcharam M Endothelial Specific Deletion of Autotaxin Improves Stroke Outcomes. Cells 2023, 12 (3). 10.3390/cells12030511.

(18). Bhattarai S; Sharma S; Ara H; Subedi U; Sun G; Li C; Bhuiyan MS; Kevil C; Armstrong WP; Minvielle MT; Miriyala S; Panchatcharam M Disrupted Blood-Brain Barrier and Mitochondrial Impairment by Autotaxin–Lysophosphatidic Acid Axis in Postischemic Stroke. J Am Heart Assoc 2021, 10 (18). 10.1161/JAHA.121.021511.

(19). Zahednasab H; Balood M; Harirchian MH; Mesbah-Namin SA; Rahimian N; Siroos B Increased Autotaxin Activity in Multiple Sclerosis. J Neuroimmunol 2014, 273 (1–2), 120–123. 10.1016/j.jneuroim.2014.06.006. [PubMed: 24984830]

(20). Schmitz K; Brunkhorst R; de Bruin N; Mayer CA; Häussler A; Ferreiros N; Schiffmann S; Parnham MJ; Tunaru S; Chun J; Offermanns S; Foerch C; Scholich K; Vogt J; Wicker S; Lötsch J; Geisslinger G; Tegeder I Dysregulation of Lysophosphatidic Acids in Multiple Sclerosis and Autoimmune Encephalomyelitis. Acta Neuropathol Commun 2017, 5 (1), 42. 10.1186/s40478-017-0446-4. [PubMed: 28578681]

(21). Nagai J; Uchida H; Matsushita Y; yano R; Ueda M; Niwa M; Aoki J; Chun J; Ueda H Autotaxin and Lysophosphatidic Acid1receptor-Mediated Demyelination of Dorsal Root Fibers by Sciatic Nerve Injury and Intrathecal Lysophosphatidylcholine. Mol Pain 2010, 6. 10.1186/1744-8069-6-78.

(22). Savaskan NE; Rocha L; Kotter MR; Baer A; Lubec G; Van Meeteren LA; Kishi Y; Aoki J; Moolenaar WH; Nitsch R; Bräuer AU Autotaxin (NPP-2) in the Brain: Cell Type-Specific Expression and Regulation during Development and after Neurotrauma. Cellular and Molecular Life Sciences 2007, 64 (2), 230–243. 10.1007/s00018-006-6412-0. [PubMed: 17192809]

(23). Ninou I; Sevastou I; Magkrioti C; Kaffe E; Stamatakis G; Thivaios S; Panayotou G; Aoki J; Kollias G; Aidinis V Genetic Deletion of Autotaxin from CD11b+ Cells Decreases the Severity of Experimental Autoimmune Encephalomyelitis. PLoS One 2020, 15 (4). 10.1371/journal.pone.0226050.

(24). Knowlden S; Georas SN The Autotaxin–LPA Axis Emerges as a Novel Regulator of Lymphocyte Homing and Inflammation. The Journal of Immunology 2014, 192 (3), 851–857. 10.4049/jimmunol.1302831. [PubMed: 24443508]

(25). Lovett-Racke AE; Rocchini AE; Choy J; Northrop SC; Hussain RZ; Ratts RB; Sikder D Silencing T-Bet Defines a Critical Role in the Differentiation of Autoreactive T Lymphocytes et Albet in Th2 Lympho-Cytes Results in IFN Production and Suppression of Th2; 2004; Vol. 21.

(26). Gocke AR; Cravens PD; Ben L-H; Hussain RZ; Northrop SC; Racke MK; Lovett-Racke AE T-Bet Regulates the Fate of Th1 and Th17 Lymphocytes in Autoimmunity. The Journal of Immunology 2007, 178 (3), 1341–1348. 10.4049/jimmunol.178.3.1341. [PubMed: 17237380]

(27). Albers HMHG; Dong A; Van Meeteren LA; Egan DA; Sunkara M; Van Tilburg EW; Schuurman K; Van Tellingen O; Morris AJ; Smyth SS; Moolenaar WH; Ovaa H Boronic Acid-Based Inhibitor of Autotaxin Reveals Rapid Turnover of LPA in the Circulation. Proc Natl Acad Sci U S A 2010, 107 (16), 7257–7262. 10.1073/pnas.1001529107. [PubMed: 20360563]

(28). Komiyama Y; Nakae S; Matsuki T; Nambu A; Ishigame H; Kakuta S; Sudo K; Iwakura Y IL-17 Plays an Important Role in the Development of Experimental Autoimmune Encephalomyelitis. The Journal of Immunology 2006, 177 (1), 566–573. 10.4049/jimmunol.177.1.566. [PubMed: 16785554]

(29). Olsson T Cytokines in Neuroinflammatory Disease: Role of Myelin Autoreactive T Cell Production of Interferon-Gamma; 1992.

(30). El-Behi M; Ciric B; Dai H; Yan Y; Cullimore M; Safavi F; Zhang GX; Dittel BN; Rostami A The Encephalitogenicity of TH 17 Cells Is Dependent on IL-1- and IL-23-Induced Production of the Cytokine GM-CSF. Nat Immunol 2011, 12 (6), 568–575. 10.1038/ni.2031. [PubMed: 21516111]

(31). Miao Y; Zhao Y; Han L; Ma X; Deng J; Yang J; Lü S; Shao F; Kong W; Wang W; Xu Q; Wang X; Feng J NSun2 Regulates Aneurysm Formation by Promoting Autotaxin Expression and T Cell Recruitment. Cellular and Molecular Life Sciences 2021, 78 (4), 1709–1727. 10.1007/s00018-020-03607-7. [PubMed: 32734582]

(32). Thirunavukkarasu K; Tan B; Swearingen CA; Rocha G; Bui HH; McCann DJ; Jones SB; Norman BH; Pfeifer LA; Saha JK Pharmacological Characterization of a Potent Inhibitor of Autotaxin in Animal Models of Inflammatory Bowel Disease and Multiple Sclerosis. Journal of Pharmacology and Experimental Therapeutics 2016, 359 (1), 207–214. 10.1124/jpet.116.234013. [PubMed: 27516465]

(33). Milo R; Kahana E Multiple Sclerosis: Geoepidemiology, Genetics and the Environment. Autoimmunity Reviews. March 2010. 10.1016/j.autrev.2009.11.010.

(34). Papenfuss TL; Rogers CJ; Gienapp I; Yurrita M; McClain M; Damico N; Valo J; Song F; Whitacre CC Sex Differences in Experimental Autoimmune Encephalomyelitis in Multiple Murine Strains. J Neuroimmunol 2004, 150 (1–2), 59–69. 10.1016/j.jneuroim.2004.01.018. [PubMed: 15081249]

(35). Sun S; Zhang X; Lyu L; Li X; Yao S; Zhang J Autotaxin Expression Is Regulated at the Post-Transcriptional Level by the RNA-Binding Proteins HuR and AUF1. Journal of Biological Chemistry 2016, 291 (50), 25823–25836. 10.1074/jbc.M116.756908. [PubMed: 27784781]

(36). Chen J; Martindale JL; Abdelmohsen K; Kumar G; Fortina PM; Gorospe M; Rostami A; Yu S RNA-Binding Protein HuR Promotes Th17 Cell Differentiation and Can Be Targeted to Reduce Autoimmune Neuroinflammation. The Journal of Immunology 2020, 204 (8), 2076–2087. 10.4049/jimmunol.1900769. [PubMed: 32169842]

(37). Borgonetti V; Sanna MD; Lucarini L; Galeotti N Targeting the RNA-Binding Protein HuR Alleviates Neuroinflammation in Experimental Autoimmune Encephalomyelitis: Potential Therapy for Multiple Sclerosis. 10.1007/s13311-020.

(38). Parham C; Chirica M; Timans J; Vaisberg E; Travis M; Cheung J; Pflanz S; Zhang R; Singh KP; Vega F; To W; Wagner J; O'Farrell A-M; McClanahan T; Zurawski S; Hannum C; Gorman D; Rennick DM; Kastelein RA; de Waal Malefyt R; Moore KW A Receptor for the Heterodimeric Cytokine IL-23 Is Composed of IL-12Rβ1 and a Novel Cytokine Receptor Subunit, IL-23R. The Journal of Immunology 2002, 168 (11), 5699–5708. 10.4049/jimmunol.168.11.5699. [PubMed: 12023369]

(39). Thompson AJ; Banwell BL; Barkhof F; Carroll WM; Coetzee T; Comi G; Correale J; Fazekas F; Filippi M; Freedman MS; Fujihara K; Galetta SL; Hartung HP; Kappos L; Lublin FD; Marrie RA; Miller AE; Miller DH; Montalban X; Mowry EM; Sorensen PS; Tintoré M; Traboulsee AL; Trojano M; Uitdehaag BMJ; Vukusic S; Waubant E; Weinshenker BG; Reingold SC; Cohen JA Diagnosis of Multiple Sclerosis: 2017 Revisions of the McDonald Criteria. The Lancet Neurology. Lancet Publishing Group February 1, 2018, pp 162–173. 10.1016/S1474-4422(17)30470-2. [PubMed: 29275977]

(40). On NH; Savant S; Toews M; Miller DW Rapid and Reversible Enhancement of Blood-Brain Barrier Permeability Using Lysophosphatidic Acid. Journal of Cerebral Blood Flow and Metabolism 2013, 33 (12), 1944–1954. 10.1038/jcbfm.2013.154. [PubMed: 24045401]

(41). Hutchinson M Natalizumab: A New Treatment for Relapsing Remitting Multiple Sclerosis; 2007; Vol. 3.

(42). Fulkerson Z; Wu T; Sunkara M; Kooi C. Vander; Morris AJ; Smyth SS Binding of Autotaxin to Integrins Localizes Lysophosphatidic Acid Production to Platelets and Mammalian Cells. Journal of Biological Chemistry 2011, 286 (40), 34654–34663. 10.1074/jbc.M111.276725. [PubMed: 21832043]

(43). Kanda H; Newton R; Klein R; Morita Y; Gunn MD; Rosen SD Autotaxin, an Ectoenzyme That Produces Lysophosphatidic Acid, Promotes the Entry of Lymphocytes into Secondary Lymphoid Organs. Nat Immunol 2008, 9 (4), 415–423. 10.1038/ni1573. [PubMed: 18327261]

(44). Uranbileg B; Ito N; Kurano M; Kano K; Uchida K; Sumitani M; Aoki J; Yatomi Y Inhibition of Autotaxin Activity Ameliorates Neuropathic Pain Derived from Lumbar Spinal Canal Stenosis. Sci Rep 2021, 11 (1). 10.1038/s41598-021-83569-3.

(45). Wheeler NA; Lister JA; Fuss B The Autotaxin–Lysophosphatidic Acid Axis Modulates Histone Acetylation and Gene Expression during Oligodendrocyte Differentiation. Journal of Neuroscience 2015, 35 (32), 11399–11414. 10.1523/JNEUROSCI.0345-15.2015. [PubMed: 26269646]

(46). Fuss B; Baba H; Phan T; Tuohy VK; Macklin WB Phosphodiesterase I, A Novel Adhesion Molecule and/or Cytokine Involved in Oligodendrocyte Function; 1997.

(47). Koike S; Keino-Masu K; Ohto T; Masu M The N-Terminal Hydrophobic Sequence of Autotaxin (ENPP2) Functions as a Signal Peptide. Genes to Cells 2006, 11 (2), 133–142. 10.1111/j.1365-2443.2006.00924.x. [PubMed: 16436050]

(48). Strominger I; Elyahu Y; Berner O; Reckhow J; Mittal K; Nemirovsky A; Monsonego A The Choroid Plexus Functions as a Niche for T-Cell Stimulation within the Central Nervous System. Front Immunol 2018, 9 (MAY). 10.3389/fimmu.2018.01066.

(49). De Graaf MT; Sillevis Smitt PAE; Luitwieler RL; Van Velzen C; Van Den Broek PDM; Kraan J; Gratama JW Central Memory CD4+ T Cells Dominate the Normal Cerebrospinal Fluid. Cytometry B Clin Cytom 2011, 80 B (1), 43–50. 10.1002/cyto.b.20542. [PubMed: 20632412]

(50). Reboldi A; Coisne C; Baumjohann D; Benvenuto F; Bottinelli D; Lira S; Uccelli A; Lanzavecchia A; Engelhardt B; Sallusto F C-C Chemokine Receptor 6-Regulated Entry of TH-17 Cells into the CNS through the Choroid Plexus Is Required for the Initiation of EAE. Nat Immunol 2009, 10 (5), 514–523. 10.1038/ni.1716. [PubMed: 19305396]

(51). Knowlden SA; Capece T; Popovic M; Chapman TJ; Rezaee F; Kim M; Georas SN Regulation of T Cell Motility in Vitro and in Vivo by LPA and LPA2. PLoS One 2014, 9 (7). 10.1371/journal.pone.0101655.

(52). Goverman J; Woods A; Larson L; Weiner LP; Hood L; Zallert DM Transgenic Mice That Express a Myelin Basic Protein-Specific T Cell Receptor Develop Spontaneous Autoimmunity; 1993; Vol. 72.

(53). Cossarizza A; Chang HD; Radbruch A; Acs A; Adam D; Adam-Klages S; Agace WW; Aghaeepour N; Akdis M; Allez M; Almeida LN; Alvisi G; Anderson G; Andrä I; Annunziato

F; Anselmo A; Bacher P; Baldari CT; Bari S; Barnaba V; Barros-Martins J; Battistini L; Bauer W; Baumgart S; Baumgarth N; Baumjohann D; Baying B; Bebawy M; Becher B; Beisker W; Benes V; Beyaert R; Blanco A; Boardman DA; Bogdan C; Borger JG; Borsellino G; Boulais PE; Bradford JA; Brenner D; Brinkman RR; Brooks AES; Busch DH; Büscher M; Bushnell TP; Calzetti F; Cameron G; Cammarata I; Cao X; Cardell SL; Casola S; Cassatella MA; Cavani A; Celada A; Chatenoud L; Chattopadhyay PK; Chow S; Christakou E; Čičin-Šain L; Clerici M; Colombo FS; Cook L; Cooke A; Cooper AM; Corbett AJ; Cosma A; Cosmi L; Coulie PG; Cumano A; Cvetkovic L; Dang VD; Dang-Heine C; Davey MS; Davies D; De Biasi S; Del Zotto G; Dela Cruz GV; Delacher M; Della Bella S; Dellabona P; Deniz G; Dessing M; Di Santo JP; Diefenbach A; Dieli F; Dolf A; Dörner T; Dress RJ; Dudziak D; Dustin M; Dutertre CA; Ebner F; Eckle SBG; Edinger M; Eede P; Ehrhardt GRA; Eich M; Engel P; Engelhardt B; Erdei A; Esser C; Everts B; Evrard M; Falk CS; Fehniger TA; Felipo-Benavent M; Ferry H; Feuerer M; Filby A; Filkor K; Fillatreau S; Follo M; Förster I; Foster J; Foulds GA; Frehse B; Frenette PS; Frischbutter S; Fritzsche W; Galbraith DW; Gangaev A; Garbi N; Gaudilliere B; Gazzinelli RT; Geginat J; Gerner W; Gherardin NA; Ghoreschi K; Gibellini L; Ginhoux F; Goda K; Godfrey DI; Goettlinger C; González-Navajas JM; Goodyear CS; Gori A; Grogan JL; Grummitt D; Grützkau A; Haftmann C; Hahn J; Hammad H; Hämmerling G; Hansmann L; Hansson G; Harpur CM; Hartmann S; Hauser A; Hauser AE; Haviland DL; Hedley D; Hernández DC; Herrera G; Herrmann M; Hess C; Höfer T; Hoffmann P; Hogquist K; Holland T; Höllt T; Holmdahl R; Hombrink P; Houston JP; Hoyer BF; Huang B; Huang FP; Huber JE; Huehn J; Hundemer M; Hunter CA; Hwang WYK; Iannone A; Ingelfinger F; Ivison SM; Jäck HM; Jani PK; Jávega B; Jonjic S; Kaiser T; Kalina T; Kamradt T; Kaufmann SHE; Keller B; Ketelaars SLC; Khalilnezhad A; Khan S; Kisielow J; Klenerman P; Knopf J; Koay HF; Kobow K; Kolls JK; Kong WT; Kopf M; Korn T; Kriegsmann K; Kristyanto H; Kroneis T; Krueger A; Kühne J; Kukat C; Kunkel D; Kunze-Schumacher H; Kurosaki T; Kurts C; Kvistborg P; Kwok I; Landry J; Lantz O; Lanuti P; LaRosa F; Lehuen A; LeibundGut-Landmann S; Leipold MD; Leung LYT; Levings MK; Lino AC; Liotta F; Litwin V; Liu Y; Ljunggren HG; Lohoff M; Lombardi G; Lopez L; López-Botet M; Lovett-Racke AE; Lubberts E; Luche H; Ludewig B; Lugli E; Lunemann S; Maecker HT; Maggi L; Maguire O; Mair F; Mair KH; Mantovani A; Manz RA; Marshall AJ; Martínez-Romero A; Martrus G; Marventano I; Maslinski W; Matarese G; Mattioli AV; Maueröder C; Mazzoni A; McCluskey J; McGrath M; McGuire HM; McInnes IB; Mei HE; Melchers F; Melzer S; Mielenz D; Miller SD; Mills KHG; Minderman H; Mjösberg J; Moore J; Moran B; Moretta L; Mosmann TR; Müller S; Multhoff G; Muñoz LE; Münz C; Nakayama T; Nasi M; Neumann K; Ng LG; Niedobitek A; Nourshargh S; Núñez G; O'Connor JE; Ochel A; Oja A; Ordonez D; Orfao A; Orlowski-Oliver E; Ouyang W; Oxenius A; Palankar R; Panse I; Pattanapanyasat K; Paulsen M; Pavlinic D; Penter L; Peterson P; Peth C; Petriz J; Piancone F; Pickl WF; Piconese S; Pinti M; Pockley AG; Podolska MJ; Poon Z; Pracht K; Prinz I; Pucillo CEM; Quataert SA; Quatrini L; Quinn KM; Radbruch H; Radstake TRDJ; Rahmig S; Rahn HP; Rajwa B; Ravichandran G; Raz Y; Rebhahn JA; Recktenwald D; Reimer D; Reis e Sousa C; Remmerswaal EBM; Richter L; Rico LG; Riddell A; Rieger AM; Robinson JP; Romagnani C; Rubartelli A; Ruland J; Saalmüller A; Saeys Y; Saito T; Sakaguchi S; Sala-de-Oyanguren F; Samstag Y; Sanderson S; Sandrock I; Santoni A; Sanz RB; Saresella M; Sautes-Fridman C; Sawitzki B; Schadt L; Scheffold A; Scherer HU; Schiemann M; Schildberg FA; Schimisky E; Schlitzer A; Schlosser J; Schmid S; Schmitt S; Schober K; Schraivogel D; Schuh W; Schüler T; Schulte R; Schulz AR; Schulz SR; Scottá C; Scott-Algara D; Sester DP; Shankey TV; Silva-Santos B; Simon AK; Sitnik KM; Sozzani S; Speiser DE; Spidlen J; Stahlberg A; Stall AM; Stanley N; Stark R; Stehle C; Steinmetz T; Stockinger H; Takahama Y; Takeda K; Tan L; Tárnok A; Tiegs G; Toldi G; Tornack J; Traggiai E; Trebak M; Tree TIM; Trotter J; Trowsdale J; Tsoumakidou M; Ulrich H; Urbanczyk S; van de Veen W; van den Broek M; van der Pol E; Van Gassen S; Van Isterdael G; van Lier RAW; Veldhoen M; Vento-Asturias S; Vieira P; Voehringer D; Volk HD; von Borstel A; von Volkmann K; Waisman A; Walker RV; Wallace PK; Wang SA; Wang XM; Ward MD; Ward-Hartstonge KA; Warnatz K; Warnes G; Warth S; Waskow C; Watson JV; Watzl C; Wegener L; Weisenburger T; Wiedemann A; Wienands J; Wilharm A; Wilkinson RJ; Willimsky G; Wing JB; Winkelmann R; Winkler TH; Wirz OF; Wong A; Wurst P; Yang JHM; Yang J; Yazdanbakhsh M; Yu L; Yue A; Zhang H; Zhao Y; Ziegler SM; Zielinski C; Zimmermann J; Zychlinsky A Guidelines for the Use of Flow Cytometry and Cell Sorting in Immunological

Studies (Second Edition). Eur J Immunol 2019, 49 (10), 1457–1973. 10.1002/eji.201970107. [PubMed: 31633216]

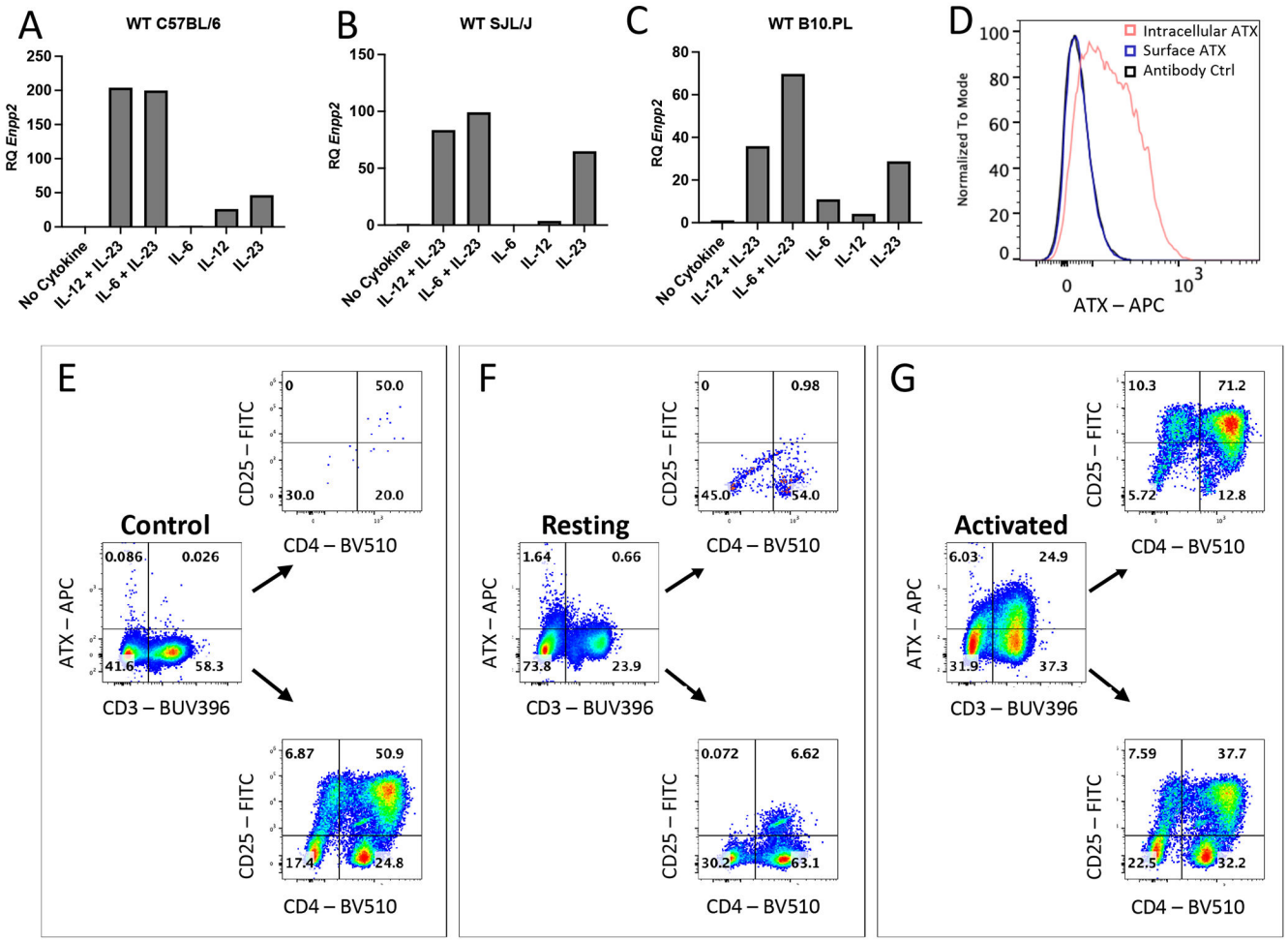

Figure 1. Increased autotaxin expression in encephalitogenic T cells *in vitro*.

A-C) RT-qPCR for *Enpp2* in CD4+ T cells from WT C57Bl/6J (A), WT SJL/J (B), and WT B10.PL (C) mouse lines that were polyclonally activated with 1μg/mL of plate-bound anti-CD3 and anti-CD28 and treated with IL-6, IL-12, and/or IL-23 *in vitro* for 3 days. RQ represents $2^{-\Delta\Delta CT}$ values calculated from endogenous loading controls. D-G) Myelin-specific splenocytes from TCR Vα2.3 Vβ8.2 mice[52] were plated 1:10 with WT B10.PL splenocytes and activated with 10μg/mL MBP Ac1-11 for 3 days. D) Histogram of ATX expression in live singlets gated on CD3+CD4+, normalized to mode. Red= intracellular ATX staining, blue= surface ATX staining, black= secondary antibody only. E-G) Dot plots depict live singlets gated on ATX and CD3 expression in cells stained with secondary antibody only (E), or resting (F) and antigen activated cells (G) stained for intracellular autotaxin. ATX+CD3+ or ATX-CD3+ cells were then gated on CD4 and CD25 to show percentage of activated CD4+ T cells. Data representative of two independent experiments.

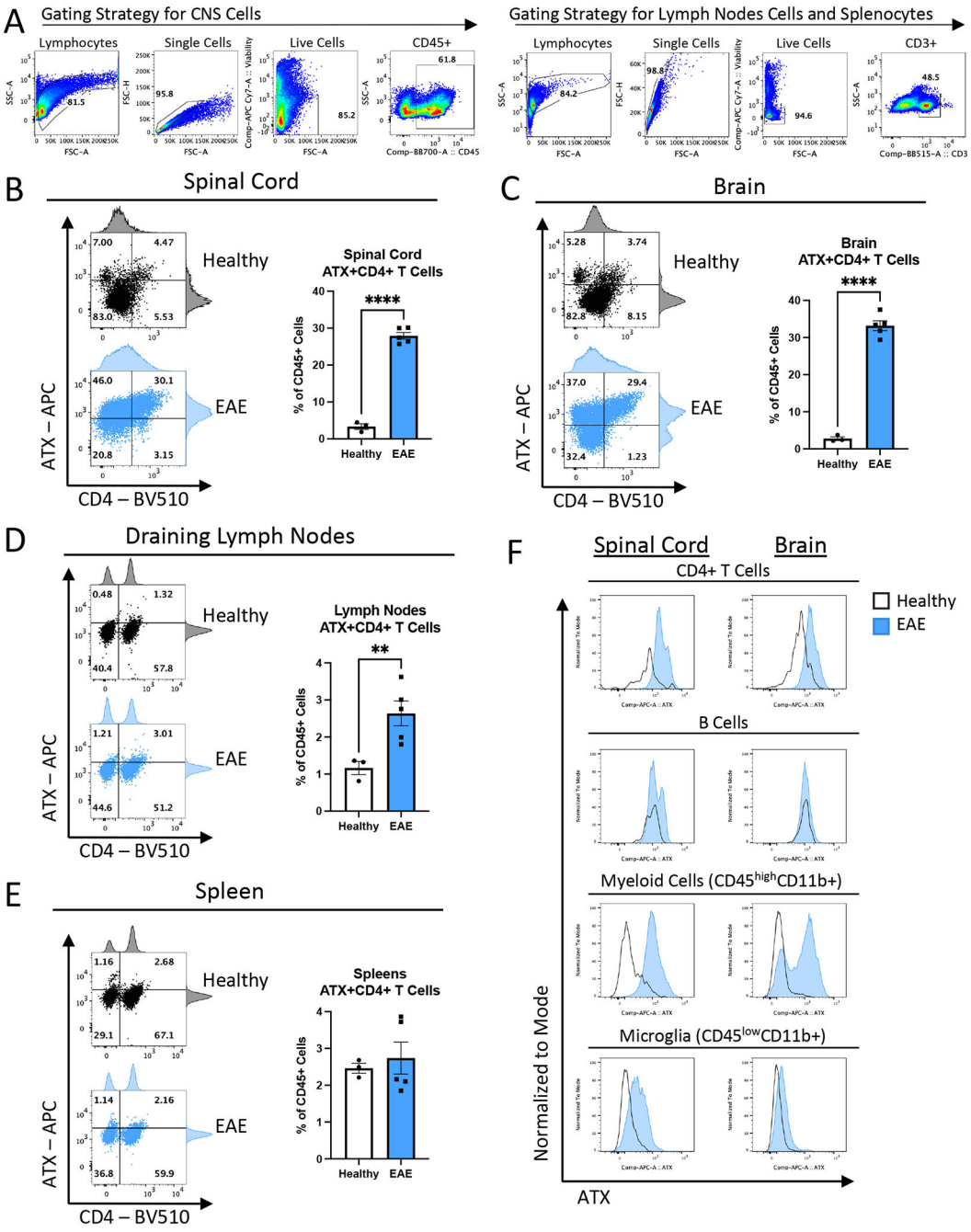

Figure 2: Autotaxin is increased by CNS infiltrating CD4+ T cells during EAE.

SJL/J mice were immunized for EAE and brains, spinal cords, draining lymph nodes, and spleens were taken on day 16 post immunization when mice showed clinical scores of 4. Immune cells were isolated as single cell suspensions and stained for flow cytometry. A) Gating strategies for CNS infiltrating immune cells (left) and peripheral immune cells (right) in healthy and EAE mice. B-E) Representative dot plots and quantification of intracellular ATX and CD4 expression on immune cells in (B) spinal cord ($p<0.0001$), (C) brain ($p=0.0024$), (D) draining lymph nodes ($p=0.0090$), and (E) spleen ($p=0.5686$).

Dot plots show data from one representative mouse per group, black= healthy, blue= EAE. Bar graphs show percentage of CD45+ cells (CNS samples) or CD3+ cells (lymph nodes and spleens) that are ATX+CD4+ from all replicates, healthy (n=3 mice), EAE (n=5 mice). Unpaired Welch's T test, ** denotes $p<0.005$, *** $p<0.0005$, **** $p<0.0001$, mean ± SEM. F) Representative histograms showing ATX expression in CD4+ T cells, B cells, myeloid cells ($CD45^{hi}CD11b+$), and microglia ($CD45^{low}CD11b+$) in brain and spinal cord samples. White= healthy, blue= EAE. Histograms normalized to mode. Data representative of two independent experiments.

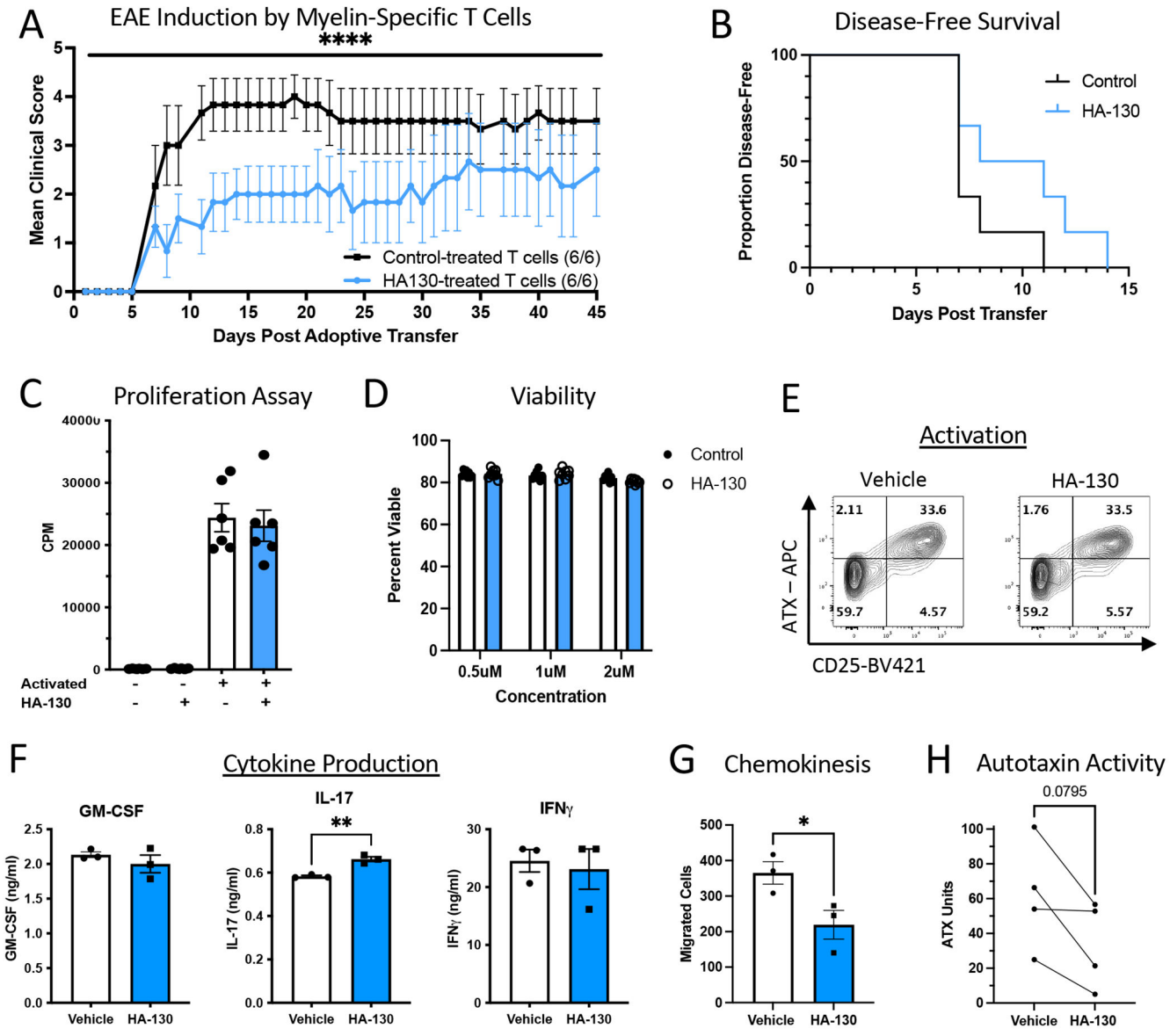

Figure 3: Autotaxin inhibition reduces T cell encephalitogenicity and *in vitro* T cell motility.

A) Mean clinical scores of EAE mice after adoptive transfer of activated, myelin-specific TCR Vα2.3 Vβ8.2 T cells that were treated with HA-130 (1μM) or vehicle for 4hr *in vitro* prior to injection into recipient mice. Number of mice that developed EAE in each group shown in parentheses. Mean + SEM, $p<0.001$, Mann-Whitney test. B) Disease-free survival of mice shown as proportion disease-free over time. Proliferation assay (C) and viability (D) of myelin specific T cells after *in vitro* activation, treatment with HA-130 (1μM for proliferation assay; 0.5, 1, or 2μM for viability assay) or vehicle. Six samples plated per condition for proliferation assay, mean ± SEM , $p>0.05$, unpaired t-test. Eight samples plated for viability assay and data are shown as percent viable, mean ± SEM , $p>0.05$, paired t-test. E) Contour plots of CD3+CD4+ T cells showing ATX and CD25 expression after 3 days of activation. Cells were activated the same as above in the presence of vehicle or HA-130 (1μM). Cells were gated by lymphocytes, single cells, live cells, and

CD3+CD4+. F) Cytokine production of myelin-specific T cells after antigen activation and *in vitro* treatment with HA-130 (1μM) or vehicle for 3 days. Samples plated in triplicate, mean ± SEM. GM-CSF (*p>0.05*), IFNγ (*p>0.05*), IL-17 (*p=0.009*), Welch's T test. G) Myelin-specific splenocytes from TCR Vα2.3 Vβ8.2 mice[52] were plated 1:10 with WT B10.PL splenocytes and activated with 10μg/mL MBP Ac1-11 for 24hr in the presence of HA-130 (1μM). Cells were collected and replated in serum free media in the top well of a Transwell plate. HA-130 or vehicle added to top well with the cells, and serum free media was added to the bottom well. Samples incubated for 20hr in incubator, and then cells that migrated into the bottom well were collected and counted. Samples ran in triplicate, mean ± SEM, Unpaired T test with Welch's correction. H) Autotaxin activity assay of cultured T cells. CD4+ T cells were isolated from 4 WT C57Bl/6J mice and polyclonally activated in the presence of IL-12 + IL-23 for 48hr. Cells were then collected, washed, and replated in serum free media for 24hr with 1μM HA-130 or vehicle. Supernatants were collected and analyzed for ATX activity. Each dot represents the average of duplicate points for one mouse. Paired T test with Welch's correction. * denotes $p<0.05$, ** $p<0.005$, *** $p<0.0005$, **** $p<0.0001$. All data representative of two or more independent experiments.

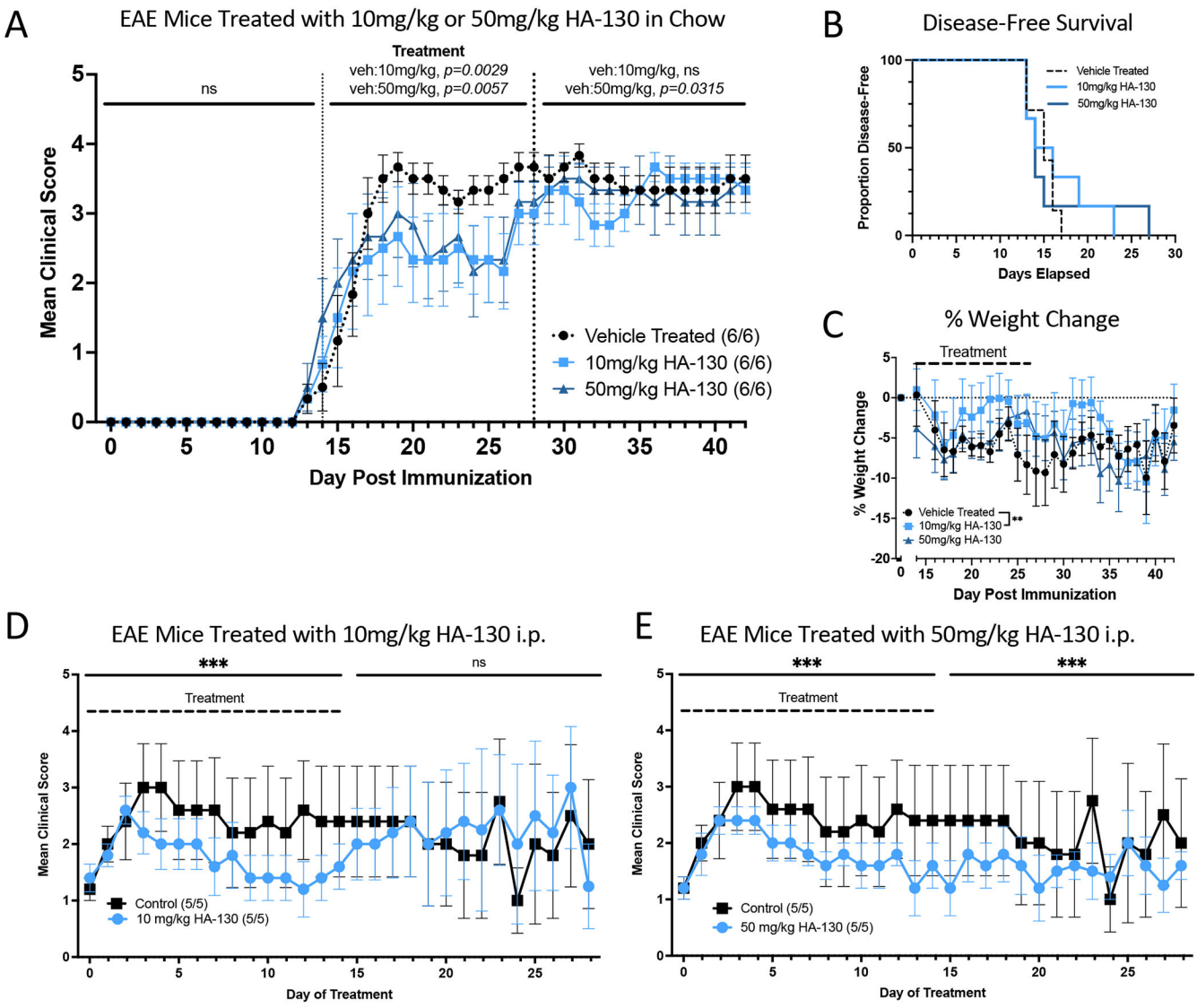

Figure 4. HA-130 decreases EAE severity at disease onset in WT C57Bl/6J mice. Female WT C57Bl/6J mice were immunized for EAE and treated with HA-130 at disease onset.

A) Mean clinical scores of EAE mice treated with vehicle, 10mg/kg HA-130, or 50mg/kg in chow for 14 days, 24hr after onset of EAE. Before treatment (*p>0.05*), during treatment (vehicle:10mg/kg, *p= 0.0029;* vehicle:50mg/kg, *p=0.0057*), after treatment (vehicle:10mg/kg, *p>0.05;* vehicle:50mg/kg, *p=0.0315*). N=6/group, mean ± SEM, Mann-Whitney. B) Disease-free survival of mice shown as proportion disease-free over time. C) Weight loss shown as percent weight change from starting weight during and after treatment. During treatment (vehicle:10mg/kg, *p= 0.0036;* vehicle:50mg/kg, *p=0.2699*), after treatment (vehicle:10mg/kg, *p=0.0682;* vehicle:50mg/kg, *p=0.7600*), mean ± SEM. D,E) Mean clinical scores of EAE mice treated 10mg/kg HA-130 (D) or 50mg/kg HA-130 (E) administered *i.p.* 24hr after disease onset. Data normalized to day 0 of treatment for each mouse. N=5/group, mean ± SEM, Mann-Whitney. During treatment (vehicle:10mg/kg, *p= 0.0002;* vehicle:50mg/kg, *p=0.0005*), after treatment (vehicle:10mg/kg, *p=0.4015;* vehicle:50mg/kg,

p=0.0001). “ns” denotes non-significant, * denotes p<0.05, ** p<0.005, *** p <0.0005, **** p<0.0001. Data representative of three independent experiments.

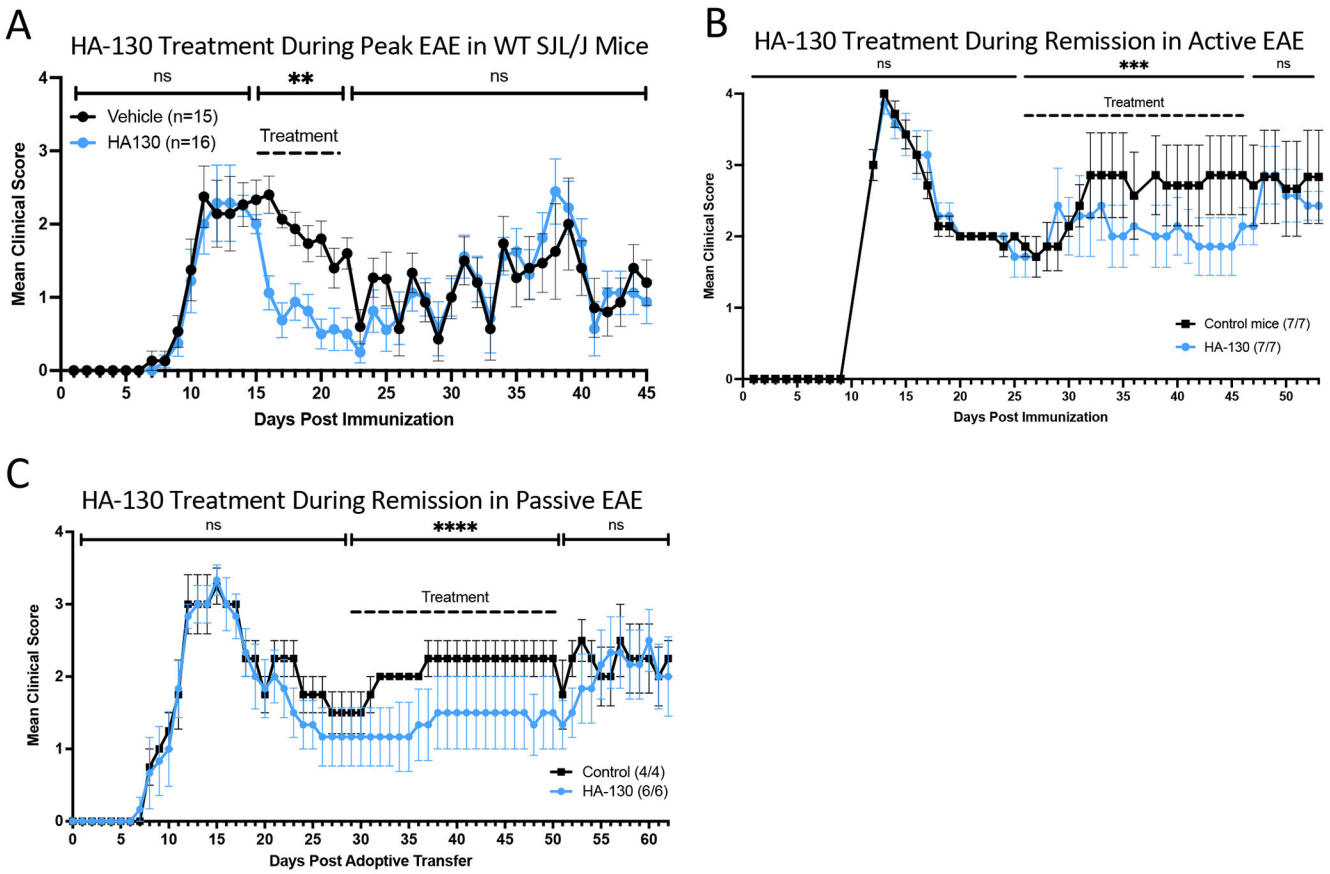

Figure 5: HA-130 treatment decreases EAE severity at peak disease and prior to first relapse in WT SJL/J mice.

A) Mean clinical scores of EAE mice treated with HA-130 (10mg/kg) or vehicle for 7 days during peak disease. Sample size shown in parenthesis. Prior to treatment (*p=0.5102*), during treatment (*p= 0.0070*), after treatment (*p=0.5841*), mean ± SEM, Mann-Whitney. B) Mean scores of mice immunized for EAE and treated with HA-130 (10mg/kg) or vehicle *i.p.* for 3 weeks during remission. Prior to treatment (*p=0.9253*), during treatment (*p= 0.0001*), after treatment (*p=0.3680*), mean ± SEM, Mann-Whitney. C) Mean clinical scores of mice treated with HA-130 (10mg/kg) or vehicle *i.p.* during remission in adoptive transfer EAE model. Donor mice were immunized with PLP 139-151/CFA and draining lymph nodes collected on day 10. Lymph node cells were isolated and activated *ex vivo* with PLP 139-151 (10μg/mL) for 3 days and then $30X10^6$ cells were injected *i.p.* into recipient mice. Mice were treated with HA-130 or vehicle *i.p.* for 3 weeks during remission. Prior to treatment (*p=0.4436*), during treatment (*p= <0.0001*), after treatment (*p=0.2087*), mean ± SEM, Mann-Whitney. "ns" denotes non-significant, * denotes p<0.05, ** p<0.005, *** p <0.0005, **** p<0.0001. Data representative of two or more independent experiments.

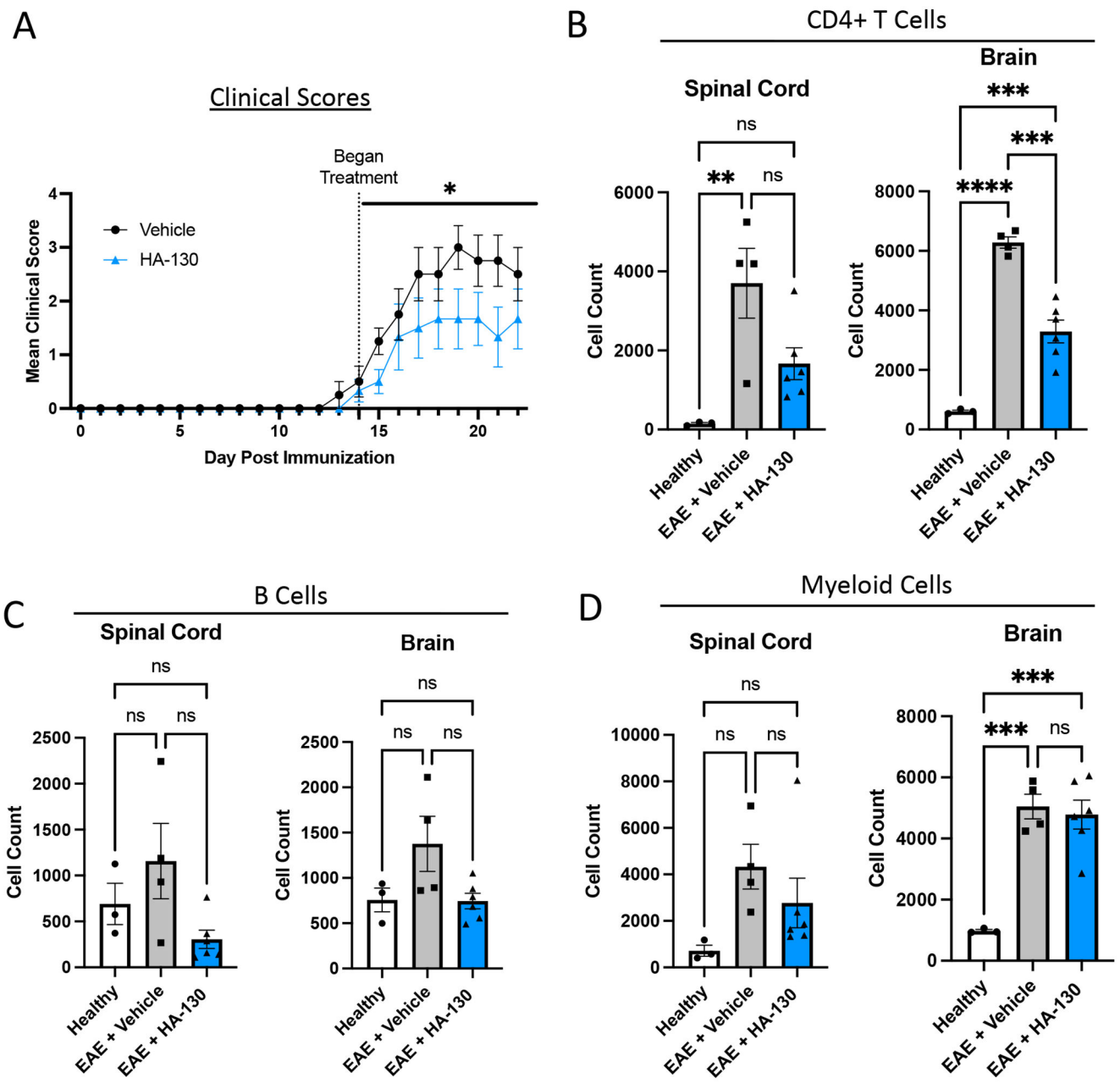

Figure 6. Autotaxin inhibition decreases number of CNS infiltrating CD4+ T cells. Female WT C57Bl/6J mice were immunized for EAE and treated with 10mg/kg HA-130 in chow at disease onset.

On day 22 post immunization, brains and spinal cords were collected and CNS infiltrating immune cells were isolated and stained for flow cytometry. A) Mean clinical scores of EAE mice, n= 4/vehicle, n=6/HA-130, mean ± SEM, Mann-Whitney (*p=0.0188*). Number of CNS infiltrating B) CD4+ T cells, C) B cells, and D) myeloid cells (all gated on live singlets). One-way ANOVA with Tukey's test for multiple comparisons, mean ± SEM; "ns" denotes non-significant, * denotes p<0.05, ** p<0.005, *** p <0.0005, **** p<0.0001. All data representative of two independent experiments.

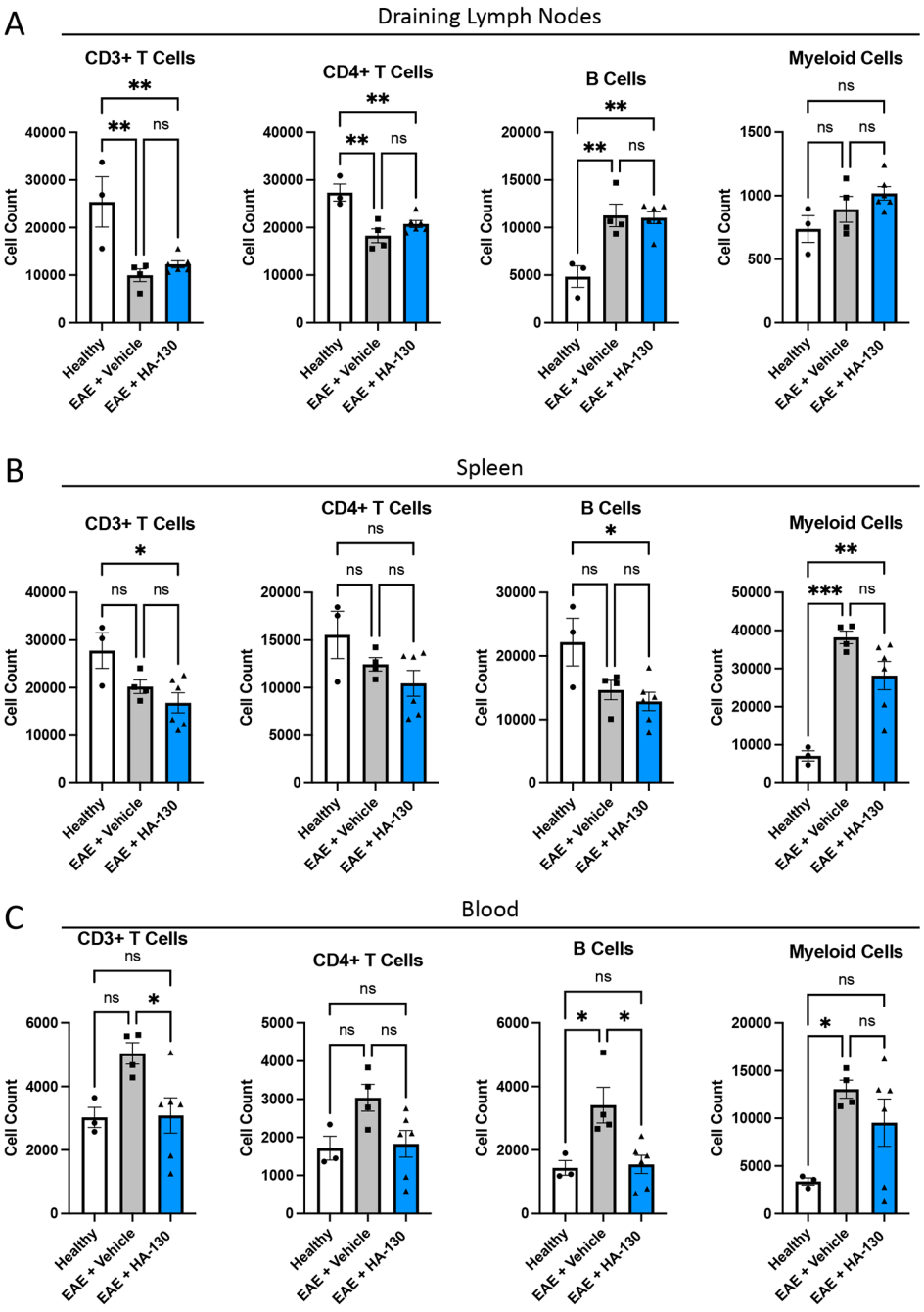

Figure 7. HA-130 changes the number of circulating immune cell populations during EAE.

Female WT C57Bl/6J mice were immunized for EAE and treated with 10mg/kg HA-130 in chow at disease onset. On day 22 post immunization, immunization site draining lymph nodes, spleens, and blood were collected and stained for flow cytometry. A-C) Number of CD3+ T cells, CD4+ T cells, B cells, or myeloid cells (all gated on live, singlets) in the A) Draining lymph nodes, B) spleen, and C) blood. N=3/healthy, n= 4/vehicle, n=6/HA-130, mean ± SEM, one-way ANOVA with Tukey's test for multiple comparisons; "ns" denotes

non-significant, * p<0.05, ** p<0.005, *** p <0.0005, **** p<0.0001. Representative of two independent experiments.